crystals

MDPI

Article

A Tunable Zig-Zag Reflective Elastic Metasurface

Zhu-Long Xu [1], Shi-Bo Yu [1], Junjie Liu [2] and Kuo-Chih Chuang [1,*]

1 Key Laboratory of Soft Machines and Smart Devices of Zhejiang Province, Institute of Applied Mechanics, School of Aeronautics and Astronautics, Zhejiang University, Hangzhou 310027, China
2 Applied Mechanics and Structure Safety Key Laboratory of Sichuan Province, School of Mechanics and Aerospace Engineering, Southwest Jiaotong University, Chengdu 610031, China
* Correspondence: chuangkc@zju.edu.cn

Abstract: In this paper, inspired by origami structures, we offer a very simple tuning method to overcome the limitations of general elastic metasurfaces, where only a certain functionality at a certain frequency range can be achieved, by designing a reflective metasurface based on foldable/deployable zig-zag structures. By utilizing peg/screw connections, the folding angles of the zig-zag structures can be easily tuned while also being fixable. By tuning the folding angle, the subunit of the zig-zag metasurface can cover a 2π phase shift span and the phase shift can be tuned continuously, and almost linearly, with respect to the folding angle. With a simple folding motion, the tunable reflective metasurface can steer reflected flexural waves in different directions and focus-reflected flexural waves with different focal distances. In addition to demonstrating tunable performance, the mechanism that associates the changing speed of the phase shift is explained. The proposed tunable zig-zag elastic metasurface provides a new way to design reconfigurable metamaterials/metasurfaces.

Keywords: tunable metasurfaces; focusing; steering; zig-zag structures

check for updates

Citation: Xu, Z.-L.; Yu, S.-B.; Liu, J.; Chuang, K.-C. A Tunable Zig-Zag Reflective Elastic Metasurface. *Crystals* **2022**, *12*, 1170. https://doi.org/10.3390/cryst12081170

Academic Editor: George Kenanakis

Received: 29 July 2022
Accepted: 16 August 2022
Published: 20 August 2022

1. Introduction

The development of metasurfaces has attracted increasing research interest due to their ultrathin and low-loss features [1–5]. As a kind of planar metamaterial, metasurfaces are composed of a series of functional elements that can manipulate wavefronts by abruptly shifting the phase and/or amplitude of waves. Although amplitude modulation is essential in some applications (e.g., holography) [6–8], various unique functionalities can still be achieved with only phase modulation. For metasurfaces with only the phase shift, also referred to as the phase gradient metasurfaces, the generalized Snell's law (GSL) [9] that relates the phase gradient profile to the corresponding transmitted or reflected wave pattern, is the most widely used design principle of metasurfaces due to its simplicity.

Different designs of elastic metasurfaces have been proposed and various functionalities, such as asymmetric transmission [10], absorption [11], steering [12,13], focusing [2,14], modal conversion [15,16], and splitting [17], of elastic waves have been achieved. However, most published metasurfaces operate only at a certain frequency to perform a certain functionality. To overcome the limitations of the narrow working frequency range and to extend their applications beyond a single functionality, several tunable metasurfaces have been proposed in which "tunability" was achieved by designing the reconfigurable mechanical elements [18–21], rotating the entire metasurfaces [22], or introducing smart materials [23–25]. Chen et al. [18] designed an acoustic metasurface with tunable hybrid resonance elements consisting of Helmholtz resonators (HRs) with moving sliders whose cavity size can be tuned by adjusting the position of the moving sliders. Similarly, Tian et al. [19] realized a programmable acoustic metasurface by changing the cavity size of the HRs and pumping fluid into/out of the unit cell. Li et al. [24] proposed an adaptive piezoelectric-based reflective acoustic metasurface. They arranged piezoelectric transducers to tailor the strength of each cavity-type membrane unit and accordingly the desired phase profile along the acoustic metasurface can be accurately achieved. Popa et al. [23] designed an active acoustic metasurface and achieved real-time control by controlling the states of piezoelectric membranes.

Although many methods and structures have been proposed to realize the tunability of acoustic metasurfaces, research on tunable metasurfaces for elastic waves is still scarce. Tang et al. [25] proposed a smart elastic metasurface composed of arrays of piezoelectric units connected with negative capacitance elements to tune the phase profiles along the metasurfaces by adjusting the negative capacitances. Similarly, Lim et al. [26,27] proposed a functionally switchable 3-bit elastic metasurface to achieve the desired phase profiles along the metasurfaces by tuning the corresponding negative capacitances of the stacked piezoelectric patches. Wang et al. [20,28] proposed a reconfigurable fish-bone elastic metasurface, where six pairs of screw bolts with equal length and two rows of nuts as vibrators are employed to construct the metasurface. In their design, the phase of the transmitted elastic waves can be tuned continuously by changing the position of the nuts by screwing them in or out.

As a common class of engineering structures generally having fixed shapes once being fabricated, zig-zag structures have been recently employed in the design of elastic metasurfaces for asymmetric transmission [29], wave steering and focusing [3], waveguides [30], and source illusion devices [31]. Combined with the concept of origami, zig-zag structures can be foldable/deployable where their shapes can change easily due to the existence of the creases. Nanda and Karami [32] designed a deployable metamaterial based on zig-zag structures and studied its tunable bandgaps. Chuang et al. [33] studied the coupling of flexural waves and longitudinal waves in zig-zag origami metamaterials and they experimentally validated the coupling phenomenon of zig-zag structures by comparing the numerical results.

In this paper, based on the zig-zag structures and the GSL, a tunable reflective elastic metasurface that can switch between different functionalities, specifically steering and focusing of the elastic waves, is studied. The tunable reflective elastic metasurface is composed of an array of deployable/foldable zig-zag structures with different folding angles. By tuning the folding angles of the zig-zag structures, the phase shift of the reflected waves can be tuned and the switchable functionalities can be achieved. Following the introduction, Section 2 describes the reflection characteristics of the subunit for the tunable reflective elastic metasurface composed of the foldable zig-zag structures. The design of the tunable zig-zag reflective elastic metasurface and the switchable functionalities are presented in Section 3. Finally, the conclusions are drawn in Section 4.

2. Reflection Characteristics of the Subunit of the Tunable Zig-Zag Reflective Elastic Metasurface

As shown in Figure 1a, the proposed tunable reflective elastic metasurface is composed of a series of zig-zag structures with different folding angles. Different folding angles lead to different flexural rigidities of the zig-zag structures and thus a desired phase shift can be achieved by folding the zig-zag structures to the prescribed angles. By tuning the folding angles, the reflective elastic metasurface can steer the reflected flexural waves in different directions and focus on the reflected flexural waves with different focal distances. We first study the reflection characteristics of the reflected flexural waves in the subunit when the zig-zag structures have different folding angles. The subunit of the tunable reflective elastic metasurface and the enlarged view of the zig-zag structures are shown in Figure 1b,c. To realize folding of the zig-zag structures, the adjacent panels are connected to each other by pegs/screws. Thus, one can change the folding angles easily while fixing the folding angles on demand by tightening the pegs/screws.

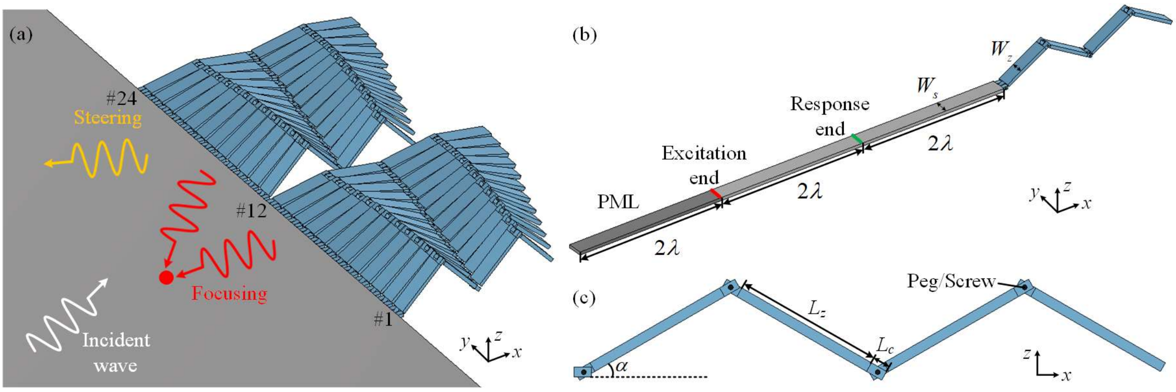

Figure 1. (**a**) Model of the tunable zig-zag reflective elastic metasurface. (**b**) Model of a subunit of the tunable zig-zag reflective elastic metasurface. (**c**) Enlarged view of the zig-zag structure with a folding angle α. # means the subunit number.

To obtain the reflection characteristics, including the phase shift and amplitude of the reflected flexural waves in the subunit, a three-dimensional finite element model is constructed in the COMSOL software. As shown in Figure 1b, a perfectly matched layer (PML) is arranged at the left-hand side of the subunit to avoid the reflection of elastic waves from the left boundary and continuity boundary conditions are applied on the lateral boundaries. Flexural wave is excited by applying a unity force along the z-direction at the excitation end (red line) and the out-of-plane z-direction displacement is picked at the response end (green line), as shown in Figure 1b. It should be noted that the picked displacement w_a includes the contributions of both the incident flexural wave w_i and the reflected flexural wave w_r, where $w_r = w_a - w_i$. Thus, another zig-zag-free model is constructed to extract the incident flexural wave w_i. The amplitude of the reflected flexural wave is $r = |w_r/w_i|$ and the phase shift $\Delta\varphi$ of the reflected flexural wave can be obtained as

$$\Delta\varphi = \begin{cases} \arctan\left(\dfrac{\mathrm{Im}(\frac{w_r}{w_i})}{\mathrm{Re}(\frac{w_r}{w_i})}\right) + \dfrac{\pi}{2} & \mathrm{Re}(\frac{w_r}{w_i}) > 0 \\ \arctan\left(\dfrac{\mathrm{Im}(\frac{w_r}{w_i})}{\mathrm{Re}(\frac{w_r}{w_i})}\right) + \dfrac{\pi}{2} + \pi & \mathrm{Re}(\frac{w_r}{w_i}) < 0 \end{cases} \tag{1}$$

.

In this paper, the length of the zig-zag structure panel L_z is set as 30 mm and the width of the zig-zag structure panel W_z is 8 mm. The length of the peg/screw connection L_c is 4 mm. The width of the subunit of the host plate W_p is 10 mm. The zig-zag structure and the host plate have the same thickness of 2 mm. The host plate and the zig-zag structures are made of aluminum with a Young's modulus of 70 GPa, a density of 2700 kg/m^3 and a Poisson ratio of 0.33. To cover a 2π phase shift span, the working frequency is first chosen as 8000 Hz and the corresponding wavelength in the host plate is 49.46 mm.

As shown in Figure 2a, the phase shift and amplitude of the reflected flexural waves in the subunit when the zig-zag structures have different folding angles are plotted. The range of the folding angle is between 0 and 60° and no mechanical interference will occur between the adjacent panels within this operation range. It is seen that the phase shift can cover a 2π span, meaning that one can easily realize a phase gradient elastic metasurface by folding the simple zig-zag structures to different angles and the phase shift changes almost linearly with respect to the folding angle, which is beneficial to the design of elastic metasurfaces. However, unlike the previously published reflective elastic metasurfaces [2], where the amplitude of the reflected wave is maintained at unity, the amplitude of the reflected flexural wave in our design is only unity at certain folding angles due to the coupling between the flexural wave and longitudinal wave caused by the asymmetry of the zig-zag structures [33]. To verify this, as shown in Figure 2b, the amplitude of the reflected longitudinal wave with respect to the folding angles is plotted. A lower amplitude of the reflected flexural wave corresponds to a higher amplitude of the reflected longitudinal wave, indicating that the reflected flexural wave at some folding angles is mitigated by the coupling between the flexural wave and the longitudinal one.

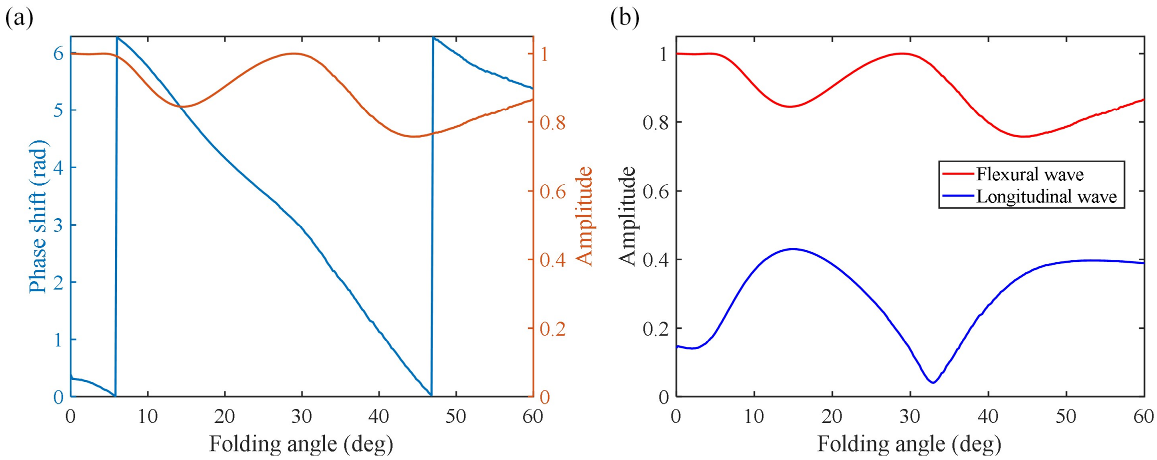

Figure 2. (**a**) Phase shift and amplitude of the reflected flexural wave and (**b**) amplitude of the reflected flexural wave and reflected longitudinal wave for the zig-zag structures with different folding angles at 8000 Hz obtained from the numerical simulations.

Then, to illustrate that the proposed reflective elastic metasurface can work at other frequencies, another two operating frequencies, 10,000 Hz and 12,000 Hz, are chosen and the phase shift and amplitude with respect to the folding angles are plotted in Figure 3. Although the working frequency has changed, the phase shift can still cover a 2π span by only tuning the folding angles, showing that the proposed reflective elastic metasurface can also work at other frequencies. However, when the working frequency increases, the phase shift changes more rapidly within a smaller folding angle range. Within the other folding angle range, the phase shift changes very slowly, which is unfavorable for practical operations. In fact, there are two regions within which the phase shift changes slowly, one in the small folding angle region and the other in the large folding angle region, and the reasons for these phenomena are different. For the small folding angle region, the phase shift change is slow due to the fact that the value of $\cos\varphi$ changes much more slowly than the one in the large folding angle. The length of the zig-zag structure projected on the x-direction is proportional to $\cos\varphi$ and the length of the zig-zag structure projected on the x-direction directly contributes to the phase shift. To verify this, the phase shift with respect to $\cos\varphi$ at three frequencies is plotted in Figure 4a. For the small folding angle region (i.e., $\cos\varphi$ is between 0.9 and 1), the phase shift also changes considerably, as shown in Figure 4a. To explain the slow phase shift change in the large folding angle region, the z-direction displacement in the right-hand side is picked and the frequency response is plotted in Figure 4b. As described in [32,33], the increasing of the folding angle will result in wider bandgaps. As shown in Figure 4b, the bandgap (i.e., the low transmission region) almost coincides with the slow-changing region of the phase shift, verifying that the low phase shift change is caused by the presence of the bandgaps in the large folding angle region. By comparing the results at 8000 Hz and the results at 10,000 Hz and 12,000 Hz, which are located within the bandgaps with respect to the larger folding angles, the presence of the bandgaps is unfavorable for the trigger of phase shifts. Although a rapid/slow change in the phase shift will bring disadvantages in practical applications, the proposed elastic metasurface composed of the zig-zag structures can still work at these frequencies.

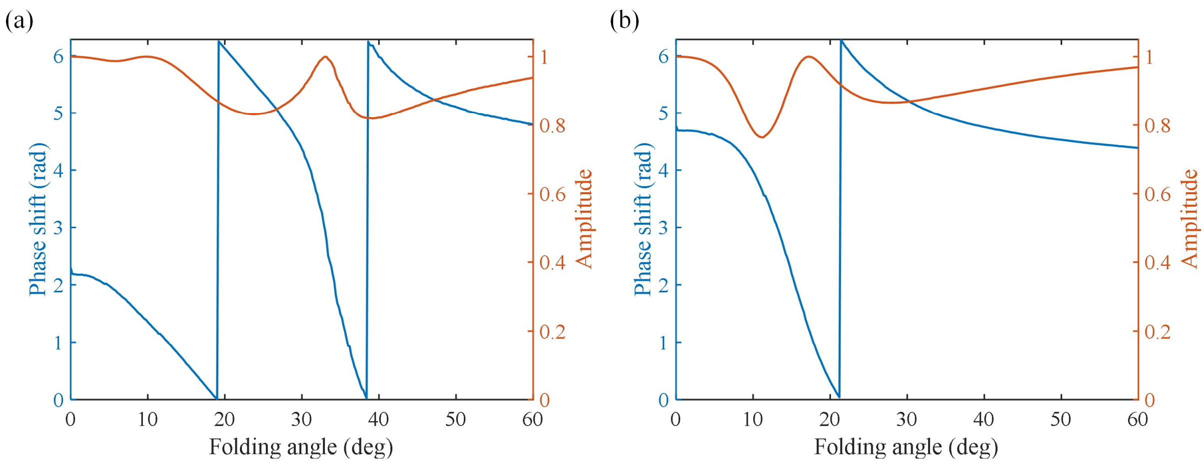

Figure 3. Phase shift and amplitude of the reflected flexural wave for the zig-zag structures with different folding angles at (**a**) 10,000 Hz and (**b**) 12,000 Hz obtained from the numerical simulations.

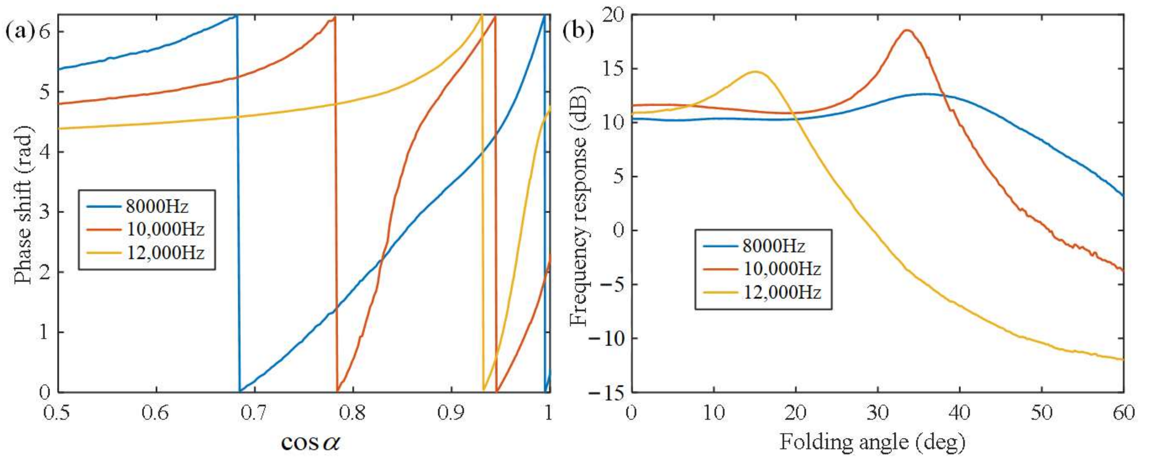

Figure 4. (**a**) The phase shift with respect to cos α at the three frequencies obtained from the numerical simulations. (**b**) Frequency response with respect to the folding angle at the three frequencies obtained from the numerical simulations.

It is shown from the above analysis that, different from the general elastic metasurfaces, where the phase shift of one subunit is fixed at a frequency and cannot be changed once being fabricated, the proposed elastic metasurface composed of the foldable zig-zag structures can tune the phase shift of each subunit to a desired one by simply tuning the folding angles.

3. Flexural Wave Manipulation Utilizing the Tunable Zig-Zag Reflective Elastic Metasurface

After analyzing the reflection characteristics of the subunit of the tunable elastic metasurface, we then design a reflective elastic metasurface to manipulate the flexural waves based on the GSL. In this section, two functionalities, steering and focusing the flexural waves, will be presented to demonstrate that the reflective elastic metasurface can work with different tunable functionalities (specifically for tuning the steering angle and focal distance).

3.1. Steering-Reflected Flexural Waves

First, the reflective elastic metasurface is designed to steer the reflected flexural waves. According to the GSL, the theoretical reflection angle can be obtained as

$$\sin\theta_r = \sin\theta_i + \frac{\lambda}{2\pi}\frac{d\phi}{dy} = \sin\theta_i + \frac{\lambda}{2\pi}\frac{2\pi}{nW_s} \tag{2}$$

where θ_r is the reflection angle, θ_i is the incident angle, $d\phi/dy$ is the spatial phase shift gradient, n is the number of the subunit to cover a 2π phase shift and W_s is the width of the subunit. A vertical incident flexural wave impinging on the tunable reflective elastic metasurface ($\theta_i = 0$) is considered. We first choose n as 12 and the corresponding phase shift distribution and folding angle distribution are shown in Figure 5a. The subunit number is numbered from small to large along the positive y-direction, as shown in Figure 1a. In this case, the theoretical reflection angle can be obtained as 24.34°. To verify the steering of reflected flexural waves in the plate, a time domain simulation is conducted in the COMSOL software. The flexural wave fields in terms of the out-of-plane displacements are plotted in Figure 5b. As a comparison, the flexural wave field on the plate without the zig-zag structures is also plotted in Figure 5c. Due to the presence of the metasurface, the direction of the reflected flexural waves has been changed and the reflection angle almost maintains as the theoretical one.

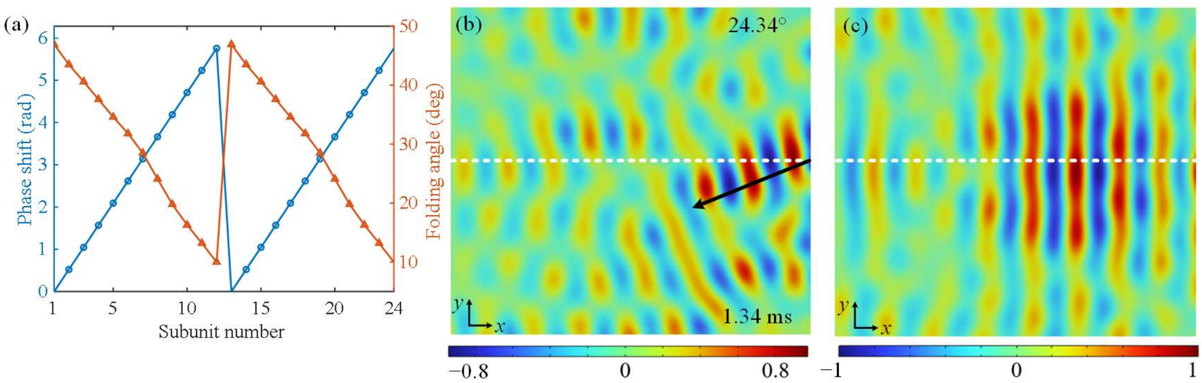

Figure 5. (**a**) Distribution of the phase shift obtained from the GSL and the distribution of the folding angle obtained from the numerical simulations in the metasurface. (**b**) Numerical simulation results of the reflected flexural wave field when n is 12 at 8000 Hz. (**c**) Numerical simulation results of the reflected flexural wave field without the metasurface at 8000 Hz.

To illustrate the tunability of the proposed metasurface, the value of n is changed to 24 and 6, and the reflection angle is changed accordingly to 11.89° and 55.51°, respectively. As shown in Figure 6, the flexural wave fields, as well as the distribution of the phase shifts and folding angles under the two cases, are plotted. It can be seen that the reflection angle of the flexural waves has changed and the results match well with the theoretical prediction. By tuning the folding angles of the zig-zag structures, the proposed reflective elastic metasurface can steer flexural waves to different directions.

3.2. Focusing Reflected Flexural Waves

After demonstrating that the tunable reflective elastic metasurface can steer the reflected flexural waves to different directions, we next show that the reflective elastic metasurface can focus the reflected flexural waves and the focal distance can be tuned. According to the GSL, the phase profile should meet the following hyperbolic secant distribution to focus a wave:

$$\phi(y) = \frac{2\pi}{\lambda}\left(\sqrt{F^2 + y^2} - F\right), \tag{3}$$

where F is the focal distance and λ is the wavelength. The focal distance is first chosen as λ and the corresponding distribution of phase shift and folding angle are shown in Figure 7a. As shown in Figure 8, the flexural wave field and the normalized energy intensity field are plotted. The focusing of the reflected flexural waves can be clearly observed. To determine the focal distance, the normalized energy intensity distribution along the longitudinal and transverse dashed lines is plotted in Figure 8c,d, respectively. It can be clearly seen that the peak of the normalized energy intensity occurs approximately at the targeted focal distance.

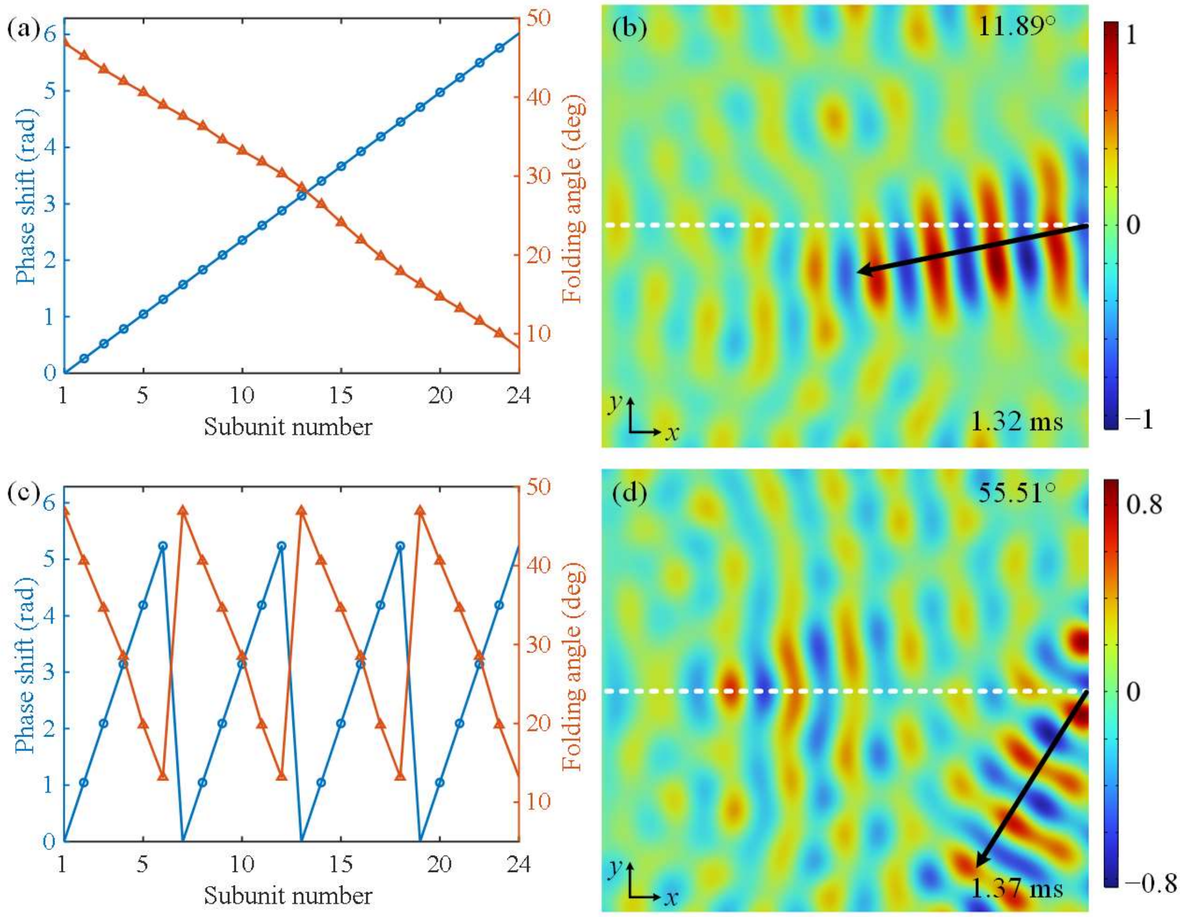

Figure 6. (**a**) Distribution of the phase shift obtained from the GSL and the distribution of the folding angle obtained from the numerical simulations in the metasurface and (**b**) numerical simulation results of the reflected flexural wave field when n is 24 at 8000 Hz. (**c**) Distribution of the phase shift obtained from the GSL and the distribution of the folding angle obtained from the numerical simulations in the metasurface and (**d**) numerical simulation results of the reflected flexural wave field when n is 6 at 8000 Hz.

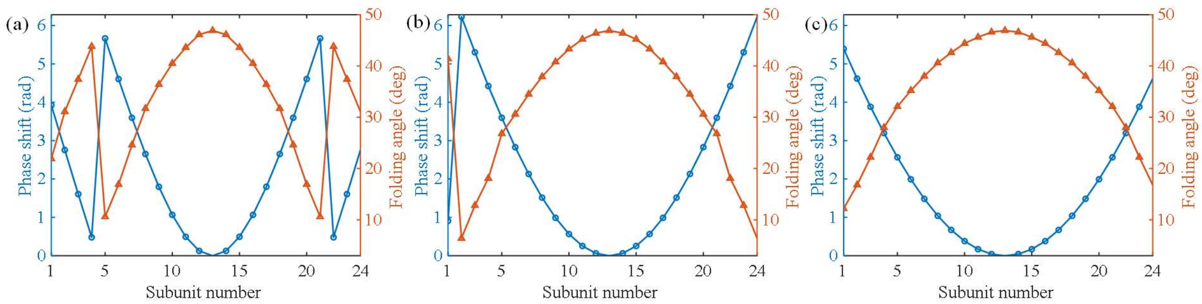

Figure 7. Distribution of the phase shift obtained from the GSL and the distribution of the folding angle obtained from the numerical simulations when the focal distance is (**a**) λ, (**b**) 2λ and (**c**) 3λ.

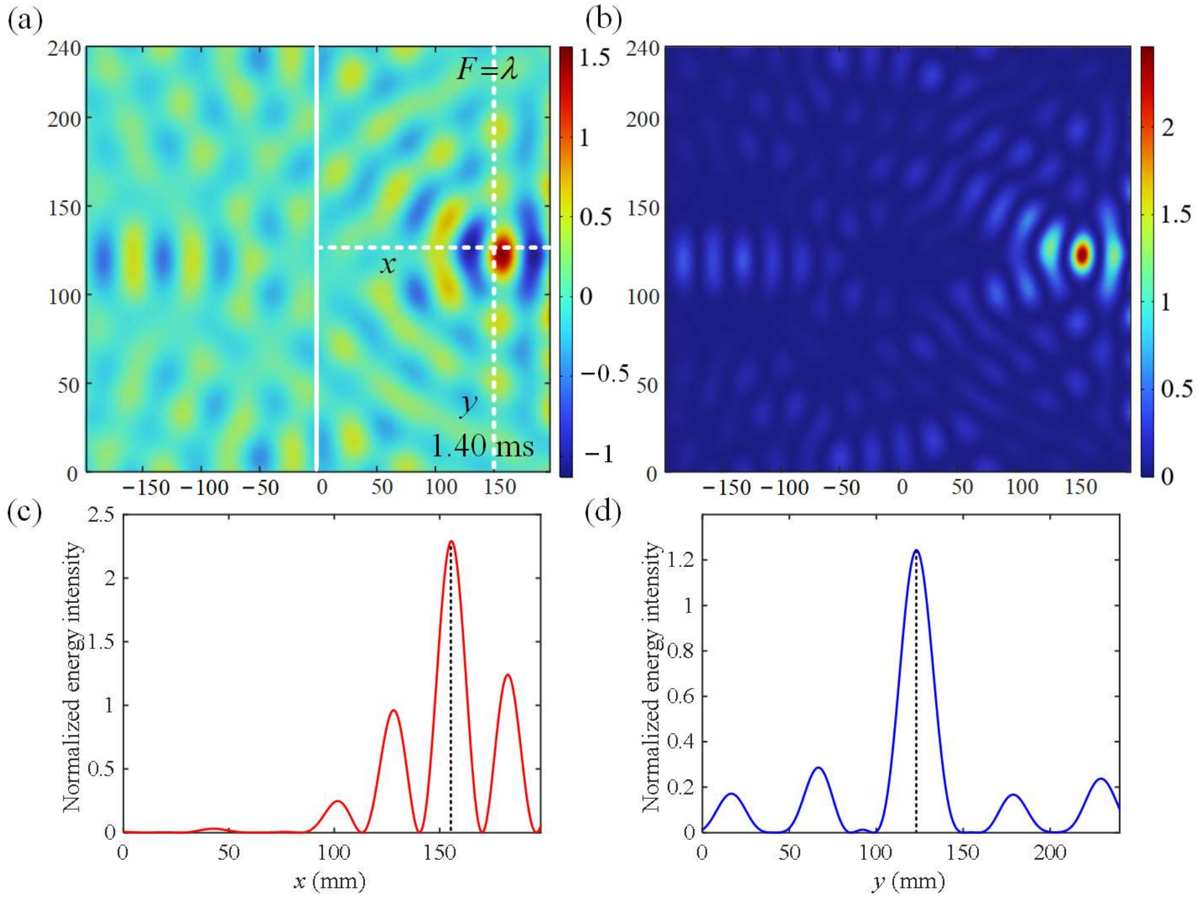

Figure 8. Numerical simulation results of (**a**) the reflected flexural wave field, (**b**) the normalized energy intensity field, and (**c**,**d**) the corresponding normalized energy intensity distribution along the white dashed line when the focal distance is λ.

Further, the focal distance is changed as 2λ and 3λ. The corresponding distributions of the phase shifts and folding angles are plotted in Figure 7b,c. To clearly observe the shifting of the focal distance, the reflected flexural wave field, the normalized energy intensity field, and the normalized energy intensity distribution along the longitudinal and transverse dashed lines are plotted in Figure 9. The simulation results match well with the theoretical predictions. Comparing the results of the three cases, it is demonstrated that desired phase profiles can be achieved by only tuning the folding angles and the focal distance can be tuned accordingly.

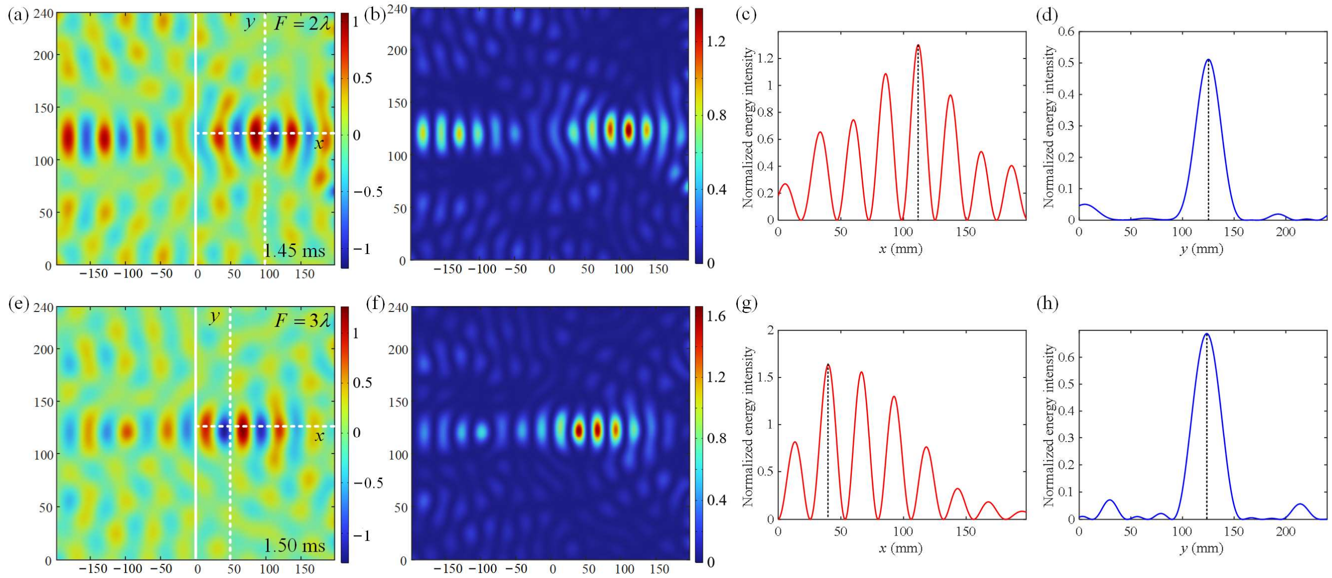

Figure 9. Numerical simulation results of (**a**) the reflected flexural wave field, (**b**) the normalized energy intensity field, and (**c**,**d**) the corresponding normalized energy intensity distribution along the white dashed line when the focal distance is 2λ. Numerical simulation results of (**e**) the reflected flexural wave field, (**f**) the normalized energy intensity field, and (**g**,**h**) the corresponding normalized energy intensity distribution along the white dashed line when the focal distance is 3λ.

4. Conclusions

In this work, a novel tunable reflective elastic metasurface composed of foldable/deployable zig-zag structures with different folding angles is proposed. By changing the folding angles of the zig-zag structures, the subunit can achieve a full 2π phase shift of the reflected flexural waves and the phase shift can change almost linearly with respect to the folding angles, which is desirable in the design of elastic metasurfaces. Inspired by the origami structures, by arranging peg/screw connections between the adjacent panels, the folding angles of the zig-zag structures can be changed and fixed easily through loosening or tightening the peg/screw units. This study shows that the presence of bandgaps is unfavorable for triggering phase shifts. Without changing other parameters of the zig-zag structures and only by tuning the folding angles, the reflective elastic metasurface can steer the reflected flexural waves to different directions and focus the flexural waves with different focal distances. Although the experimental validation is not conducted in this paper, the ability to tune the bandgaps of the foldable/deployable zig-zag structures have been validated experimentally in our previous study [33] and thus the numerical simulation results in this paper are very likely to be achieved in the experiments. In practice, if motors are arranged at the connections associated with precise feedback control, adaptive tuning of the elastic waves can be achieved utilizing the proposed zig-zag reflective elastic metasurface. The simple, in the sense of fabrication and operation, and configurable reflective elastic metasurface proposed in this paper shows great potential for flexural wave manipulation in fields such as energy harvesting, wave absorption, waveguide and especially wave mode conversion due to the intrinsic wave coupling in zig-zag structures.

Author Contributions: Formal analysis, Z.-L.X. and K.-C.C.; Funding acquisition, J.L. and K.-C.C.; Investigation, Z.-L.X.; Methodology, Z.-L.X. and K.-C.C.; Supervision, K.-C.C.; Validation, Z.-L.X.; Visualization, S.-B.Y.; Writing—original draft, Z.-L.X. and K.-C.C.; Writing—review & editing, J.L. and K.-C.C. All authors have read and agreed to the published version of the manuscript.

Funding: This research was funded by the National Natural Science Foundation of China (Nos. 11972318 and 12102370), the Opening Project of Applied Mechanics and Structure Safety Key Laboratory of Sichuan Province (No. SZDKF-202001), and the Fundamental Research Funds for the Central Universities (No. 2682021CX082).

Institutional Review Board Statement: Not applicable.

Informed Consent Statement: Not applicable.

Data Availability Statement: The data that support the findings of this study are available from the corresponding author upon reasonable request.

Conflicts of Interest: The authors declare no conflict of interest.

References

1. Zhu, Y.; Fan, X.; Liang, B.; Cheng, J.; Jing, Y. Ultrathin acoustic metasurface-based Schroeder diffuser. *Phys. Rev. X* **2017**, *7*, 021034. [CrossRef]
2. Zhao, T.; Yang, Z.; Tian, W.; Cao, L.; Xu, Y. Deep-subwavelength elastic metasurface with force-moment resonators for abnormally reflecting flexural waves. *Int. J. Mech. Sci.* **2022**, *221*, 107193. [CrossRef]
3. Su, G.; Zhang, Y.; Liu, Y.; Wang, T. Steering flexural waves by amplitude-shift elastic metasurfaces. *J. Appl. Mech.* **2021**, *88*, 051011. [CrossRef]
4. Zheng, G.; Mühlenbernd, H.; Kenney, M.; Li, G.; Zentgraf, T.; Zhang, S. Metasurface holograms reaching 80% efficiency. *Nat. Nanotechnol.* **2015**, *10*, 308–312. [CrossRef]
5. Chen, A.-L.; Wang, Y.-S.; Wang, Y.-F.; Zhou, H.-T.; Yuan, S.-M. Design of Acoustic/Elastic Phase Gradient Metasurfaces: Principles, Functional Elements, Tunability, and Coding. *Appl. Mech. Rev.* **2022**, *74*, 020801. [CrossRef]
6. Huang, L.; Zhang, S.; Zentgraf, T. Metasurface holography: From fundamentals to applications. *Nanophotonics* **2018**, *7*, 1169–1190. [CrossRef]
7. Deng, Z.-L.; Li, G. Metasurface optical holography. *Mater. Today Phys.* **2017**, *3*, 16–32. [CrossRef]
8. Tian, Y.; Wei, Q.; Cheng, Y.; Liu, X. Acoustic holography based on composite metasurface with decoupled modulation of phase and amplitude. *Appl. Phys. Lett.* **2017**, *110*, 191901. [CrossRef]
9. Yu, N.; Genevet, P.; Kats, M.A.; Aieta, F.; Tetienne, J.-P.; Capasso, F.; Gaburro, Z. Light propagation with phase discontinuities: Generalized laws of reflection and refraction. *Science* **2011**, *334*, 333–337. [CrossRef]
10. Cao, L.; Xu, Y.; Assouar, B.; Yang, Z. Asymmetric flexural wave transmission based on dual-layer elastic gradient metasurfaces. *Appl. Phys. Lett.* **2018**, *113*, 183506. [CrossRef]
11. Cao, L.; Yang, Z.; Xu, Y.; Fan, S.-W.; Zhu, Y.; Chen, Z.; Li, Y.; Assouar, B. Flexural wave absorption by lossy gradient elastic metasurface. *J. Mech. Phys. Solids* **2020**, *143*, 104052. [CrossRef]
12. Zhu, H.; Semperlotti, F. Anomalous refraction of acoustic guided waves in solids with geometrically tapered metasurfaces. *Phys. Rev. Lett.* **2016**, *117*, 034302. [CrossRef] [PubMed]
13. Cao, L.; Yang, Z.; Xu, Y.; Assouar, B. Deflecting flexural wave with high transmission by using pillared elastic metasurface. *Smart. Mater. Struct.* **2018**, *27*, 075051. [CrossRef]
14. Jiang, Y.; Liu, Y.; Kou, M.; Li, H.; Wu, X.; Zeng, X.; Bi, X.; Zhang, H.; Hu, N. Multi-parameter independent manipulation for flexural wave by notched metasurface. *Int. J. Mech. Sci.* **2022**, *214*, 106928. [CrossRef]
15. Kim, M.S.; Lee, W.R.; Kim, Y.Y.; Oh, J.H. Transmodal elastic metasurface for broad angle total mode conversion. *Appl. Phys. Lett.* **2018**, *112*, 241905. [CrossRef]
16. Lee, S.W.; Seung, H.M.; Choi, W.; Kim, M.; Oh, J.H. Broad-angle refractive transmodal elastic metasurface. *Appl. Phys. Lett.* **2020**, *117*, 213502. [CrossRef]
17. Zheng, M.; Park, C.I.; Liu, X.; Zhu, R.; Hu, G.; Kim, Y.Y. Non-resonant metasurface for broadband elastic wave mode splitting. *Appl. Phys. Lett.* **2020**, *116*, 171903. [CrossRef]
18. Chen, Z.; Shao, S.; Negahban, M.; Li, Z. Tunable metasurface for acoustic wave redirection, focusing and source illusion. *J. Phys. D Appl. Phys.* **2019**, *52*, 395503. [CrossRef]
19. Tian, Z.; Shen, C.; Li, J.; Reit, E.; Gu, Y.; Fu, H.; Cummer, S.A.; Huang, T.J. Programmable acoustic metasurfaces. *Adv. Funct. Mater.* **2019**, *29*, 1808489. [CrossRef]
20. Yuan, S.-M.; Chen, A.-L.; Wang, Y.-S. Switchable multifunctional fish-bone elastic metasurface for transmitted plate wave modulation. *J. Sound Vib.* **2020**, *470*, 115168. [CrossRef]
21. Fan, S.-W.; Zhao, S.-D.; Chen, A.-L.; Wang, Y.-F.; Assouar, B.; Wang, Y.-S. Tunable broadband reflective acoustic metasurface. *Phys. Rev. Appl.* **2019**, *11*, 044038. [CrossRef]
22. Li, Y.; Shen, C.; Xie, Y.; Li, J.; Wang, W.; Cummer, S.A.; Jing, Y. Tunable asymmetric transmission via lossy acoustic metasurfaces. *Phys. Rev. Lett.* **2017**, *119*, 035501. [CrossRef] [PubMed]
23. Popa, B.-I.; Shinde, D.; Konneker, A.; Cummer, S.A. Active acoustic metamaterials reconfigurable in real time. *Phys. Rev. B* **2015**, *91*, 220303. [CrossRef]

24. Li, S.; Xu, J.; Yao, Y.; Tang, J. Tunable reflected acoustic wave front modulated with piezoelectric metasurfaces. *J. Phys. D: Appl. Phys.* **2020**, *54*, 095102. [CrossRef]
25. Li, S.; Xu, J.; Tang, J. Tunable modulation of refracted lamb wave front facilitated by adaptive elastic metasurfaces. *Appl. Phys. Lett.* **2018**, *112*, 021903. [CrossRef]
26. Yaw, Z.; Zhou, W.; Lim, C. Anomalous wave control by an adaptive elastic metasurface shunted with negative capacitance circuit. *J. Sound Vib.* **2022**, *525*, 116782. [CrossRef]
27. Yaw, Z.; Zhou, W.; Chen, Z.; Lim, C. Stiffness tuning of a functional-switchable active coding elastic metasurface. *Int. J. Mech. Sci.* **2021**, *207*, 106654. [CrossRef]
28. Yuan, S.-M.; Chen, A.-L.; Cao, L.; Zhang, H.-W.; Fan, S.-W.; Assouar, B.; Wang, Y.-S. Tunable multifunctional fish-bone elastic metasurface for the wavefront manipulation of the transmitted in-plane waves. *J. Appl. Phys.* **2020**, *128*, 224502. [CrossRef]
29. Li, B.; Hu, Y.; Chen, J.; Su, G.; Liu, Y.; Zhao, M.; Li, Z. Efficient asymmetric transmission of elastic waves in thin plates with lossless metasurfaces. *Phys. Rev. Appl.* **2020**, *14*, 054029. [CrossRef]
30. Hu, Y.; Zhang, Y.; Su, G.; Zhao, M.; Li, B.; Liu, Y.; Li, Z. Realization of ultrathin waveguides by elastic metagratings. *Commun. Phys.* **2022**, *5*, 62. [CrossRef]
31. Liu, Y.; Liang, Z.; Liu, F.; Diba, O.; Lamb, A.; Li, J. Source illusion devices for flexural lamb waves using elastic metasurfaces. *Phys. Rev. Lett.* **2017**, *119*, 034301. [CrossRef] [PubMed]
32. Nanda, A.; Karami, M.A. Tunable bandgaps in a deployable metamaterial. *J. Sound Vib.* **2018**, *424*, 120–136. [CrossRef]
33. Xu, Z.-L.; Xu, S.-F.; Chuang, K.-C. Coupled flexural-longitudinal waves in an origami metamaterial with uncoupled creases. *Phys. Lett. A* **2021**, *396*, 127232. [CrossRef]